AIAA JOURNAL
Vol. 43, No. 6, June 2005

Turbulence Correlation Length-Scale Relationships for the Prediction of Aeroacoustic Response

Denis A. Lynch III* and William K. Blake†
U.S. Naval Surface Warfare Center, West Bethesda, Maryland 20817-5700
and
Thomas J. Mueller‡
University of Notre Dame, Notre Dame, Indiana 46556-5684

Expressions to describe the correlation length scales of turbulent inflow to an aerodynamic body are derived as functions of the classic integral length scale and anisotropy correction factors. These one-point parameters are significantly easier to determine experimentally than traditional correlation-scale measurement techniques, which involve multiple probes at multiple locations. As such correlation scales are necessary to properly estimate the aeroacoustic response of the body, such a technique could have substantial benefit in a wide variety of applications. The approach is applied to a recent experimental study examining the response of a stator downstream of a propeller that is itself ingesting broadband turbulence. Results suggest that the derived expressions not only accurately represent correlation length scales, but also enable the accurate prediction of the acoustic output of the stator.

Nomenclature

C	=	chord length
f	=	temporal frequency
$\boldsymbol{i}$	=	three-dimensional vector of quantity i
i_1	=	quantity i in the freestream direction
i_2	=	quantity i in the direction normal to airfoil (stator) surface
i_3	=	quantity i in the spanwise direction of airfoil (stator) surface
i_∞	=	freestream quantity
i^*	=	complex conjugate of quantity i
k	=	wave number
L_i	=	geometric length scale
M	=	Mach number
q	=	dynamic pressure
R_{ij}	=	correlation function between turbulent velocity components u_i and u_j
r	=	separation distance between two points
$\mathcal{S}e$	=	aerodynamic response function (Sears function)
U	=	mean velocity component
u	=	turbulent velocity component
x	=	flow location (position)
α_c, β_c	=	anisotropy scaling factors
β	=	angle between acoustic source and receiver, measured with respect to dipole axis
γ^2	=	coherence function
δ	=	Dirac delta function
Λ, Λ_1	=	classic turbulence integral length scale
$\Lambda_i\|_j$	=	turbulence correlation scale of jth component of velocity in ith direction
ρ_0	=	density of fluid
Φ_{ii}	=	autopower spectrum in the ith direction
$\Phi_{ii}(\boldsymbol{r})$	=	cross-power spectrum in the ith direction (separated by distance $\boldsymbol{r}$)
$\Phi_{p_{\text{rad}}}$	=	radiated far-field acoustic pressure
$\phi_{ii}(\boldsymbol{r})$	=	nondimensional cross-spectral density function of turbulence in the ith direction (separated by distance $\boldsymbol{r}$)
ω	=	gust or event frequency ($=2\pi f$)

Presented as Paper 2002-2569 at the AIAA/CEAS 8th Aeroacoustics Conference, Breckenridge, CO, 17–19 June 2002; received 5 May 2003; revision received 17 December 2004; accepted for publication 14 January 2005.

*Acoustic Engineer, Code 7250, Hydroacoustics, Carderock Division.
†Chief Scientist, Code 7051, Hydroacoustics, Carderock Division.
‡Roth–Gibson Professor, Department of Aerospace and Mechanical Engineering. Fellow AIAA.

I. Introduction

THE relationship between broadband inflow turbulence and the aeroacoustic response of an aerodynamic body has been studied in great detail. Theoretical modeling of this response originally considered a gust interacting with a flat-plate airfoil and has grown in complexity over the years. However, the expressions still depend on several fundamental quantities, one of which is the spanwise correlation length scale of the turbulence.

In practice, the spanwise correlation length scale represents a challenge to determine experimentally. It requires two-point measurements at an infinite number of probe separation distances. It is therefore advantageous to derive an expression for this spanwise correlation length scale in terms of quantities that are more easily determined, such as the classic integral length scale.

This paper describes the theoretical derivation of such a relationship. The equations derived will then be applied to an experimental study, with the predictive capability of the theoretical relationships being analyzed. The benefit of these efforts is manifested in the accurate prediction of spanwise correlation scales used in the modeling of a body's aeroacoustic response with a minimal amount of additional time-consuming, costly measurements.

II. Derivation of Integral Correlation Length Scales

The aeroacoustic response of an airfoil responding to an unsteady gust has been well documented. The majority of this work is built directly on the pioneering efforts of von Kármán and Sears[1] and Sears.[2] In effect, the acoustic output generated by the airfoil can be accurately estimated from characteristics of the turbulent flowfield driving the response of the airfoil using derived theoretical expressions. A full explanation of this derivation is not provided here for brevity, but is given in Chapter 11 of Blake.[3] The governing equation for the acoustic output of an airfoil $\Phi_{p_{\text{rad}}}$, assuming a compact

source, is

$$\frac{\Phi_{p_{\text{rad}}}(\omega)}{q_\infty^2 M_\infty^2} = \sin^2\beta\left(\frac{\overline{u_2^2}}{U_\infty^2}\right)\left(\frac{L_3}{r}\right)^2\left(\frac{\omega C}{2U_\infty}\right)^2\phi_{22}(\omega)\frac{2\Lambda_3(\omega)|_2}{L_3} \times \left|\mathcal{S}e\left(\frac{\omega C}{2U_\infty}\right)\right|^2 \tag{1}$$

Here, almost all of these terms represent quantities that can be obtained through detailed but feasible measurements. The freestream dynamic pressure, Mach number, and velocity (q_∞, M_∞, and U_∞, respectively) are easily determined. The angle β, or angle between the acoustic measurement position and chord of the airfoil, is defined in the experimental setup. The quantities u_2^2 and $\phi_{22}(\omega)$ represent the mean square turbulence and normalized turbulence spectrum in the x_2 (normal to the airfoil) direction. (The coordinate system for all discussions in this paper is defined in Sec. II.A.) The frequency in question is represented by ω, and $\mathcal{S}e$ represents the classic Sears function.

The final two terms, L_3 and $\Lambda_3|_2$, represent contributions to the acoustic output of the system as a function of spanwise dependence. The term L_3 actually defines the span of the airfoil or airfoil section being considered, whereas $\Lambda_3|_2$ is the spanwise correlation length of the gust velocity. In other words, this term speaks to how correlated the response of the airfoil is to the gust along the spanwise direction. If the spanwise correlation is large, then the acoustic output from the unsteady pressure response of adjacent airfoil sections will sum in the far field. Likewise, if the spanwise correlation is small, then the unsteady pressure field of adjacent airfoil sections will be unrelated, greatly reducing the radiated acoustic output. It is clear that an important factor in the prediction of the unsteady pressure response (and therefore the farfield acoustic response) of a propeller blade or stator vane is the spanwise correlation length of the gust velocity $\Lambda_3|_2$.

The definition and use of this necessary length scale are not new. Beyond the presentation mentioned taken from Blake,[3] this length scale is also defined and used in works by Amiet,[4] Wygnanski et al.,[5] and Glegg.[6] It has been examined recently in much closer detail by Devenport et al.[7,8] and Glegg et al.[9] In papers such as these, the length scales in question were usually determined in one of three basic ways. First, scales could be determined using an exhaustive array of two-point velocity correlation measurements. Second, the length scales could be estimated using a relationship to some physical scale of the turbulence (such as the half-width or momentum thickness of the wake of the turbulence generating body). The final method assumes a curve shape for the turbulence spectra and adjusts the unknown but desired length scales and intensity levels to obtain a best fit of the one-point spectra measurements to the assumed shape. The goal of this paper is to express the spanwise correlation length using one-point flowfield measurements and a quasi-isotropic model with coordinate stretching to develop equations based on the classic integral length scale. In all such cases, the modeling is envisioned to apply to well-distributed fields of turbulence.

A. Extractions from Turbulence Modeling

To complete the model for the spanwise correlation of the gust velocity, a number of assumptions are made regarding the inflow turbulence. Although many of these assumptions simply do not hold for many complex flowfields, it provides a baseline for the development of the theory. Corrections will be introduced as necessary.

First, a coordinate system is defined. Here, x_1 corresponds to the streamwise direction, x_2 to the cross-stream direction normal to the aerodynamic body in question, and x_3 the cross-stream direction along the span of the aerodynamic body. The flow is aligned such that the primary direction is the same as the mean convection velocity U_c. Therefore,

$$\boldsymbol{U} = \{U_c, 0, 0\} \longrightarrow \boldsymbol{U}\cdot\boldsymbol{k} = U_1 k_1 = U_c k_1$$
$$\boldsymbol{r} = \{r_1, r_2, r_3\} \longrightarrow \boldsymbol{U}\cdot\boldsymbol{r} = U_1 r_1 = U_c r_1 \tag{2}$$

From this, the convective wave number can be defined as $k_1 = k_c = \omega/U_c$.

Next, the flow is assumed quasi-isotropic in the energy sense. The isotropic assumption means that the turbulent energy has no preferred direction and is homogeneous. However, even in cases where the flow has both preferred direction and inhomogeneities, the flow might still show some signs of isotropy.[10] Therefore, this assumption of isotropy in the energy sense is made. Expressed mathematically, this can be written

$$\overline{u_1^2} = \overline{u_2^2} = \overline{u_3^2} = \overline{u^2} \tag{3}$$

where the directions are as already defined.

Correlation length scales are based on the summation of simultaneous flow measurements at all locations. Therefore, the expression of these quantities requires both a temporal and spatial dependence. In measurements involving two sensors, generalized cross-spectral energy can be expressed as

$$\Phi_{ij}(\boldsymbol{r};\omega) = \langle u_i(\boldsymbol{r}+\boldsymbol{x};\omega)u_j^*(\boldsymbol{x};\omega)\rangle \tag{4}$$

where the subscripts i and j denote the possibility of different components (directions) of the velocity vector, the asterisk denotes the complex conjugate, $\boldsymbol{x}$ is the position of the reference sensor, and $\boldsymbol{r}$ is a vector relating the position of the second sensor relative to the reference sensor. This expression is also a function of frequency ω, obtained by Fourier transform of the measured signal expressed in the time domain. Like the temporal dependence expressed as a function of frequency, the spatial dependence can be expressed as a function of wave number by Fourier transform and vice versa. Mathematically stated,

$$\Phi_{ij}(\boldsymbol{r};\omega) = \iiint_{-\infty}^{\infty}\Phi_{ij}(\boldsymbol{k};\omega)\exp(i\boldsymbol{k}\cdot\boldsymbol{r})d^3\boldsymbol{k} \tag{5}$$

However, the expression is left in terms of sensor separation $\boldsymbol{r}$ for a moment. The primary focus of this paper is a length scale based on a spanwise separation. Therefore, for much of the paper the spatial dependence can be simplified, namely,

$$\Phi_{ij}(r_1=0, r_2=0, r_3;\omega) = \langle u_i(\boldsymbol{r}+\boldsymbol{x};\omega)u_j^*(\boldsymbol{x};\omega)\rangle \tag{6}$$

The autospectral density can be defined in the special case where $r_3 \to 0$ and $i = j$, namely,

$$\Phi_{ii}(\omega) = \langle u_i(\boldsymbol{x};\omega)u_i^*(\boldsymbol{x};\omega)\rangle = \Phi_{ii}(r_1=0, r_2=0, r_3=0;\omega) \tag{7}$$

Further, the cross-spectral density function of a given spanwise separation can be nondimensionalized using the autospectral density,

$$\phi_{ii}(r_3;\omega) = \frac{\Phi_{ii}(r_1=r_2=0, r_3;\omega)}{\Phi_{ii}(\omega)} \tag{8}$$

where $\phi_{ii}(r_3=0;\omega)=1$ and $\phi_{ii}(r_3\to\infty;\omega)<1$. Typically, ϕ_{ii} is a complex quantity.

A related assumption that comes from the assumption of quasi-isotropy in the energy sense is that the respective energy densities are also equal. It is further assumed that the energy densities are nondimensionalized such that

$$\int_{-\infty}^{\infty}\Phi_{ii}(\omega)\,\mathrm{d}\omega = 1, \qquad i = 1, 2, 3 \tag{9}$$

For the case of isotropic turbulence, a correlation function between velocity components u_i and u_j is defined as

$$\Phi_{ij}(\boldsymbol{r};\omega) = \Phi_{ij}\left(\sqrt{r_1^2+r_2^2+r_3^2};\omega\right) \tag{10}$$

Although the turbulence is defined as isotropic in the energy sense, it is certainly not so in the spatial sense. To model this anisotropy,

stretching scale factors are introduced in the definition of $\boldsymbol{r}$ such that the magnitude is expressed as

$$|\boldsymbol{r}|^2 = r^2 = r_1^2 + (r_2/\beta_c)^2 + (r_3/\alpha_c)^2 = \mathrm{r}_1^2 + \mathrm{r}_2^2 + \mathrm{r}_3^2 = \mathrm{r}^2 \quad (11)$$

where α_c and β_c are stretching parameters and r is an expression of the separation vector that incorporates the stretching parameters. These stretching parameters have been used in previous efforts to account for anisotropy in the flow.[11] Including these parameters, the energy density as a function of wave number and temporal frequency can be expressed as

$$\begin{aligned}
\Phi_{ij}(\boldsymbol{k};\omega) &= \frac{1}{(2\pi)^3}\iiint_{-\infty}^{\infty}\Phi_{ij}(\boldsymbol{r};\omega)\exp(i\boldsymbol{k}\cdot\boldsymbol{r})d^3\boldsymbol{r} \\
&= \frac{1}{(2\pi)^3}\iiint_{-\infty}^{\infty}\Phi_{ij}\left[\sqrt{r_1^2+\left(\frac{r_2}{\beta_c}\right)^2+\left(\frac{r_3}{\alpha_c}\right)^2};\omega\right] \\
&\quad\times\exp(i\boldsymbol{k}\cdot\boldsymbol{r})d^3\boldsymbol{r} \\
&= \frac{\alpha_c\beta_c}{(2\pi)^3}\iiint_{-\infty}^{\infty}\Phi_{ij}\left[\sqrt{r_1^2+\left(\frac{r_2}{\beta_c}\right)^2+\left(\frac{r_3}{\alpha_c}\right)^2};\omega\right] \\
&\quad\times\exp\left[i\left(k_1r_1+k_2\beta_c\frac{r_2}{\beta_c}+k_3\alpha_c\frac{r_3}{\alpha_c}\right)\right]\mathrm{d}r_1\,\mathrm{d}\frac{r_2}{\beta_c}\,\mathrm{d}\frac{r_3}{\alpha_c} \\
&= \frac{\alpha_c\beta_c}{(2\pi)^3}\iiint_{-\infty}^{\infty}\Phi_{ij}(\mathbf{r};\omega)\exp(i\boldsymbol{k}\cdot\boldsymbol{r})d^3\mathbf{r}
\end{aligned}$$

$$\Phi_{ij}(\boldsymbol{k}) = \alpha_c\beta_c\Phi_{ij}(\mathbf{k}) \quad (12)$$

where $\mathbf{k} = \{k_1, k_2\beta_c, k_3\alpha_c\}$ and k_1 = wave number vector component aligned with flow direction; k_2 = vertical cross-stream direction (the "gust" direction); and k_3 = spanwise cross-stream direction.

This allows $\Phi_{ij}(\mathbf{k})$ to be modeled using isotropic turbulence models. From Hinze,[12] the two-sided wave-number spectra are given as

$$\Phi_{ii}(\mathbf{k}) = \frac{2\Lambda^3}{\pi^2}\frac{\mathrm{k}^2-\mathrm{k}_i^2}{(1+\mathrm{k}^2\Lambda^2)^3} \quad (13)$$

where $i = 1, 2, 3$, Λ is the classic integral scale turbulence parameter (defined more explicitly later in this paper), and

$$\begin{aligned}
\mathrm{k}^2 &= \mathrm{k}_1^2 + \mathrm{k}_2^2 + \mathrm{k}_3^2 \\
&= k_1^2 + (\beta_c k_2)^2 + (\alpha_c k_3)^2
\end{aligned} \quad (14)$$

The combination of Eq. (12) with Eq. (13) gives, after some simplification, expressions for the energy density of velocity in all three primary directions as a function of wave numbers k_i, the classic integral length scale Λ, and stretching parameters α_c and β_c:

$$\Phi_{11}(\boldsymbol{k}) = \frac{2\alpha_c\beta_c\Lambda^3}{\pi^2}\frac{\left[(k_2\beta_c)^2+(k_3\alpha_c)^2\right]\Lambda^2}{\left\{1+\left[k_1^2+(k_2\beta_c)^2+(k_3\alpha_c)^2\right]\Lambda^2\right\}^3} \quad (15)$$

$$\Phi_{22}(\boldsymbol{k}) = \frac{2\alpha_c\beta_c\Lambda^3}{\pi^2}\frac{\left[k_1^2+(k_3\alpha_c)^2\right]\Lambda^2}{\left\{1+\left[k_1^2+(k_2\beta_c)^2+(k_3\alpha_c)^2\right]\Lambda^2\right\}^3} \quad (16)$$

$$\Phi_{33}(\boldsymbol{k}) = \frac{2\alpha_c\beta_c\Lambda^3}{\pi^2}\frac{\left[k_1^2+(k_2\beta_c)^2\right]\Lambda^2}{\left\{1+\left[k_1^2+(k_2\beta_c)^2+(k_3\alpha_c)^2\right]\Lambda^2\right\}^3} \quad (17)$$

Now that the energy density can be expressed in this fashion, attention turns to the definition of the correlation lengths in question.

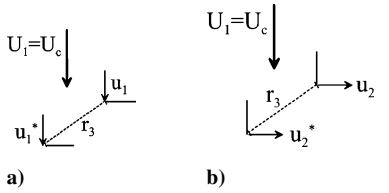

Fig. 1 Schematic comparing a) spanwise correlation of streamwise velocity u_1 and b) spanwise correlation of cross-stream velocity u_2.

Note that although related, these are not the same as the integral length scale, as discussed earlier.

An important distinction needs to be emphasized at this point. Figure 1 shows the difference between two commonly measured scales. Figure 1a depicts the spanwise correlation of the streamwise, or u_1, velocity. This is the most commonly measured correlation length in traditional turbulence measurements. However, the important correlation length in terms of the acoustic production from an airfoil or propeller, as explained in Sec. II, is the spanwise correlation of the normal gust, or u_2, component of velocity. These two components are not the same, even in the case of isotropic turbulence.

An integral correlation length scale is defined as

$$\Lambda_i(\omega)|_j = \int_0^\infty \phi_{jj}(r_i,\omega)\,\mathrm{d}r_i \quad (18)$$

The term $\Lambda_j(\omega)|_i$ can be read as "the correlation in the r_j direction of the ith component of velocity." A special case of this correlation length scale is the classic turbulence integral length scale. That is, $\phi_{jj}(r_i,\omega)$ is simply the Fourier transform of the correlation function $\phi_{jj}(r_i,t)$, often expressed in other literature as $R_{jj}(r_i,t)$. If the timescale t is dropped and $i = j$, then the resulting equation is

$$\Lambda_j = \int_0^\infty \phi_{jj}(r_j)\,\mathrm{d}r_j \quad (19)$$

To be precise, Λ_1 [defined using Eq. (19) with $j = 1$] is the turbulence integral scale of isotropic turbulence (and referred to as Λ for the remainder of this paper). This scale is the driving factor in defining turbulence energy spectra levels.[12] Other correlation length scales, as defined in the more general Eq. (18), are frequency-dependent correlation lengths, and are derived from specific integral "cuts" through the three-dimensional wave-number energy spectrum. For the current consideration, analysis is kept in the frequency domain with the frequency dependence preserved, as in the more general definition of Eq. (18).

From Eq. (18), the spanwise correlation lengths in question are now defined as

$$2\Lambda_3(\omega)|_1 = \int_{-\infty}^\infty \phi_{11}(r_3;\omega)\,\mathrm{d}r_3 \quad (20)$$

$$2\Lambda_3(\omega)|_2 = \int_{-\infty}^\infty \phi_{22}(r_3;\omega)\,\mathrm{d}r_3 \quad (21)$$

In the strictest sense, these correlation lengths can be found by finding $\Phi_{ii}(r_3,\omega)$ for an infinite set of separation distances r_3, then integrating the nondimensionalized spectral density. Obviously, this is inconvenient and could prove time consuming and costly. A simplified expression is therefore sought, one that will also allow for quasi-isotropic flows, to predict these length scales. Again, for the purposes of the unsteady response of an airfoil or propeller blade, the length scale defined in Eq. (21) is the critical term.

B. Integral Correlation Length Scales as Functions of Turbulence Integral Length Scale

Sections II.B.1–II.B.3 use the relations just defined in order to derive closed-form expressions for relevant correlation scales as

functions of frequency and turbulence integral length scale. Section II.B.1 includes a detailed derivation of the expression for spanwise correlation length of the streamwise velocity component. Because the analysis is similar, the derivation for spanwise correlation length of the normal velocity component (Sec. II.B.2) is not as detailed. Section II.B.3 defines relationships between these scales, as well as presents, without derivation, the corresponding correlation length scales in the normal direction.

1. Spanwise Correlation Length of the Streamwise Velocity Component

As the spanwise correlation of the streamwise component is the most commonly measured of these correlation lengths, it is proper to consider it first. From Eq. (20),

$$2\Lambda_3(\omega)|_1 = \int_{-\infty}^{\infty} \phi_{11}(r_3;\omega)\,\mathrm{d}r_3 = \frac{1}{\Phi_{11}(\omega)} \int_{-\infty}^{\infty} \Phi_{11}(r_1 = r_2 = 0, r_3;\omega)\,\mathrm{d}r_3 \quad (22)$$

Using a frozen-field approximation and Eq. (5), this can be expressed as

$$\Phi_{ij}(\boldsymbol{r};\omega) = \iiint_{-\infty}^{\infty} \Phi_{ij}(\boldsymbol{k};\omega)\delta(\omega - \boldsymbol{U}\cdot\boldsymbol{k}) \exp(i\boldsymbol{k}\cdot\boldsymbol{r}) d^3\boldsymbol{k} \quad (23)$$

where δ is defined as the Dirac delta function. Integrating over U_1, as that relates only to the convection velocity U_c, gives

$$\Phi_{ij}(\boldsymbol{r};\omega) = \frac{1}{U_c} \iint_{-\infty}^{\infty} \Phi_{ij}(\boldsymbol{k}') \exp(i\boldsymbol{k}'\cdot\boldsymbol{r})\,\mathrm{d}k_2\,\mathrm{d}k_3 \quad (24)$$

where $\boldsymbol{k}' = \{k_c, k_2, k_3\}$ because $k_1 = k_c = \omega/U_c$ is the convective wave number, a natural result of considering the turbulence field frozen. There is no separation in the normal direction, and so $r_2 = 0$, giving

$$\Phi_{ij}(\boldsymbol{r};\omega) = \frac{1}{U_c} \iint_{-\infty}^{\infty} \Phi_{ij}(\boldsymbol{k}') \exp(ik_3 r_3)\,\mathrm{d}k_2\,\mathrm{d}k_3 \quad (25)$$

Substitution of Eq. (25) into Eq. (22) gives

$$\Phi_{11}(\omega)2\Lambda_3(\omega)|_1 = \frac{1}{U_c} \iint_{-\infty}^{\infty} \Phi_{11}(k_c, k_2, k_3) \times \left\{ \int_{-\infty}^{\infty} \exp(ik_3 r_3)\,\mathrm{d}r_3 \right\} \mathrm{d}k_2\,\mathrm{d}k_3 \quad (26)$$

Integration over r_3 gives a result of $2\pi\delta(k_3)$, where δ is the Dirac delta function. Therefore, the resulting double integral has a nonzero value only in the case of $k_3 = 0$. The expression can be written

$$\Phi_{11}(\omega)2\Lambda_3(\omega)|_1 = \frac{2\pi}{U_c} \int_{-\infty}^{\infty} \Phi_{11}(k_c, k_2, k_3 = 0)\,\mathrm{d}k_2 \quad (27)$$

Equation (15) gives an expression for $\Phi_{11}(\boldsymbol{k})$. Substitution and simplification (for example, setting $k_3 = 0$) gives

$$\Phi_{11}(\omega)2\Lambda_3(\omega)|_1 = \frac{2\pi}{U_c} \frac{2\alpha_c\Lambda^2}{\pi^2} \int_{-\infty}^{\infty} \frac{[\beta_c k_2\Lambda]^2 d(\beta_c k_2\Lambda)}{\left[1 + (k_1\Lambda)^2 + (\beta_c k_2\Lambda)^2\right]^3} \quad (28)$$

From Gradshteyn and Ryzhik,[13]

$$\int_0^{\infty} \frac{x^2\,\mathrm{d}x}{(ax^2 + c)^3} = \frac{\pi}{16(ac)^{\frac{3}{2}}} \quad (29)$$

and so combining Eqs. (28) and (29) gives

$$\Phi_{11}(\omega)2\Lambda_3(\omega)|_1 = \frac{2\pi}{U_c}\frac{2\alpha_c\Lambda^2}{\pi^2}\frac{\pi}{8}\frac{1}{\left[1 + (k_c\Lambda)^2\right]^{\frac{3}{2}}} = \frac{\Lambda^2\alpha_c}{2U_c}\frac{1}{\left[1 + (k_c\Lambda)^2\right]^{\frac{3}{2}}} \quad (30)$$

Now, an expression for $\Phi_{11}(\omega)$ can be determined by integrating over all three wave-number domains. Employing the simplification of Eq. (24) and expression for $\Phi_{11}(\boldsymbol{k})$ of Eq. (15),

$$\begin{aligned}\Phi_{11}(\omega) &= \frac{1}{U_c} \iint_{-\infty}^{\infty} \Phi_{11}(k_c, k_2, k_3)\,\mathrm{d}k_2\,\mathrm{d}k_3 \\ &= \frac{1}{U_c}\frac{2\Lambda^3}{\pi^2}\alpha_c\beta_c \iint_{-\infty}^{\infty} \frac{\left[(k_2\beta_c)^2 + (k_3\alpha_c)^2\right]\Lambda^2\,\mathrm{d}k_2\,\mathrm{d}k_3}{\left\{1 + \left[k_c^2 + (k_2\beta_c)^2 + (k_3\alpha_c)^2\right]\Lambda^2\right\}^3} \\ &= \frac{1}{U_c}\frac{2\Lambda}{\pi^2} \iint_{-\infty}^{\infty} \frac{\left[(k_2\beta_c)^2 + (k_3\alpha_c)^2\right]\Lambda^2\,\mathrm{d}(k_2\beta_c\Lambda)\,\mathrm{d}(k_3\alpha_c\Lambda)}{\left\{1 + \left[k_c^2 + (k_2\beta_c)^2 + (k_3\alpha_c)^2\right]\Lambda^2\right\}^3}\end{aligned} \quad (31)$$

It can be shown that

$$\iint_{-\infty}^{\infty} \frac{(x^2 + y^2)\,\mathrm{d}x\,\mathrm{d}y}{[C^2 + x^2 + y^2]^3} = \frac{\pi}{2C^2} \quad (32)$$

giving the final form of $\Phi_{11}(\omega)$ as

$$\Phi_{11}(\omega) = \frac{1}{U_c}\frac{2\Lambda}{\pi^2}\frac{\pi}{2\left[1 + (k_c\Lambda)^2\right]} = \frac{\Lambda}{\pi U_c}\frac{1}{1 + (k_c\Lambda)^2} \quad (33)$$

This expression is the same as the two-sided wave-number spectrum for isotropic turbulence in the streamwise direction as defined in Hinze.[12]

Finally, Eqs. (30) and (33) can be combined to give a ratio of the spanwise correlation scale of streamwise velocity to the traditional integral length scale, namely,

$$\Lambda_3(\omega)|_1/\Lambda = (\pi\alpha_c/4)\left\{1\Big/\left[1 + (k_c\Lambda)^2\right]^{\frac{1}{2}}\right\} \quad (34)$$

This equation represents an important result in this experimental effort. The correlation scale, which is obtained by integrating the normalized u_1 cross-spectral density over the separation variable r_3, can be predicted simply by measuring the traditional integral length scale and accounting for anisotropy between the k_1 and k_3 directions using the term α_c. Although this correlation scale is commonly measured,[10] it is not the correlation scale needed to predict the unsteady surface pressure and far-field acoustic response of an airfoil or propeller in a turbulent field.

2. Spanwise Correlation Length of the Normal Velocity Component

Attention is now turned to developing a prediction for the spanwise correlation length of the normal, or gust component of velocity, used in the prediction of the aeroacoustic response of an airfoil [see Eq. (1)]. Again, it can be measured by integrating the nondimensional cross-spectral density over the separation variable r_3. From

Eq. (21) and the arguments used for Eq. (22),

$$2\Lambda_3(\omega)|_2 = \frac{1}{\Phi_{22}(\omega)} \int_{-\infty}^{\infty} \Phi_{22}(r_1 = r_2 = 0, r_3; \omega)\, \mathrm{d}r_3 \tag{35}$$

Hinze[12] shows that $\Phi_{22}(\omega)$ can also be expressed in terms of the classic turbulence length scale Λ. This expression can be written as

$$\Phi_{22}(\omega) = \frac{\Lambda}{2\pi U_c} \frac{1 + 3(k_c\Lambda)^2}{\left[1 + (k_c\Lambda)^2\right]^2} \tag{36}$$

leaving only the numerator of Eq. (35) to be determined. Using the same arguments as outlined in Eqs. (24–27) of Sec. II.B.1, k_3 is set to zero, and, after substitution of Eq. (16),

$$\Phi_{22}(\omega)2\Lambda_3(\omega)|_2 = \frac{4}{\pi U_c}\alpha_c\Lambda^2(k_c\Lambda)^2 \times \int_{-\infty}^{\infty} \frac{\mathrm{d}(k_2\beta_c\Lambda)}{\left[1 + (k_c\Lambda)^2 + (k_2\beta_c\Lambda)^2\right]^3} \tag{37}$$

Again, Gradshteyn and Ryzhik[13] show that

$$\int_{-\infty}^{\infty} \frac{\mathrm{d}x}{[ax^2 + c]^3} = \frac{3\pi}{16c^2\sqrt{ac}} \tag{38}$$

Substitution gives

$$\begin{aligned}\Phi_{22}(\omega)2\Lambda_3(\omega)|_2 &= (4/\pi U_c)\alpha_c\Lambda^2(k_c\Lambda)^2(3\pi/8) \times \left\{1/\left[1 + (k_c\Lambda)^2\right]^2\left[1 + (k_c\Lambda)^2\right]^{\frac{1}{2}}\right\} \\ &= \left(3\Lambda^2/2U_c\right)\alpha_c(k_c\Lambda)^2\left\{1/\left[1 + (k_c\Lambda)^2\right]^{\frac{5}{2}}\right\}\end{aligned} \tag{39}$$

Finally, combining Eqs. (36) and (39) gives the dimensionless spanwise correlation length of stream-normal (gust) velocity in the form just used, namely,

$$\frac{\Lambda_3(\omega)|_2}{\Lambda} = \frac{3\pi\alpha_c}{2} \frac{(k_c\Lambda)^2}{\left[1 + (k_c\Lambda)^2\right]^{\frac{1}{2}}\left[1 + 3(k_c\Lambda)^2\right]} \tag{40}$$

This is the crucial correlation length needed for predicting the acoustic output of the airfoil. Subject to assumption of a nearly homogeneous turbulent field, this frequency-dependent correlation length scale is now expressed as a function of two constants, α_c and Λ, and convective wave number k_c. Experimental examination of this result can be made by measuring this length scale in the traditional sense. The ratio of $\Lambda_3(\omega)|_2$ to Λ [derived as Eq. (40)] is presented in Fig. 2 for $\alpha_c = 1$. As will be shown in Sec. IV.B and IV.C, even results for highly complex turbulent flowfields collapse to this uniform curve.

3. Additional Correlation Scale Relationships

As $\Lambda_3(\omega)|_1$ is often measured experimentally or estimated, a relationship between the two scales is also useful:

$$\begin{aligned}\frac{\Lambda_3(\omega)|_2}{\Lambda_3(\omega)|_1} &= \frac{\Lambda_3(\omega)|_2}{\Lambda} \times \frac{\Lambda}{\Lambda_3(\omega)|_1} \\ &= \frac{6(k_c\Lambda)^2}{\left[1 + 3(k_c\Lambda)^2\right]}\end{aligned} \tag{41}$$

For completeness (although not used in this investigation), similar correlation lengths in the normal direction can be found for these same velocity components. Using the notation just defined,

$$\frac{\Lambda_2(\omega)|_1}{\Lambda} = \frac{\pi\beta_c}{4} \frac{1}{\left[1 + (k_c\Lambda)^2\right]^{\frac{1}{2}}} \tag{42}$$

$$\frac{\Lambda_2(\omega)|_2}{\Lambda} = \frac{3\pi\beta_c}{2} \frac{(k_c\Lambda)^2}{\left[1 + (k_c\Lambda)^2\right]^{\frac{1}{2}}\left[1 + 3(k_c\Lambda)^2\right]} \tag{43}$$

which are, respectively, the correlation lengths of u_1 and u_2 velocities in the stream-normal separation direction. Note that in the limit of isotropic turbulence, $\alpha_c = \beta_c$, $\Lambda_2(\omega)|_2 = \Lambda_3(\omega)|_2$, $\Lambda_2(\omega)|_1 = \Lambda_3(\omega)|_1$.

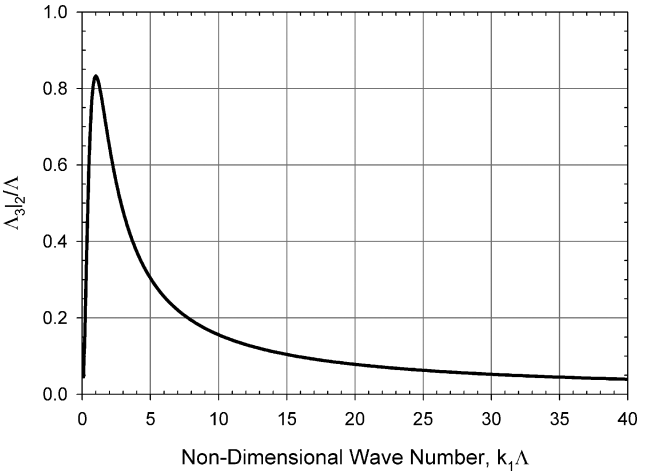

Fig. 2 Ratio of correlation length scale $\Lambda_3|_2$ to integral length scale Λ.

III. Experimental Setup

A series of experiments were completed in order to examine the effectiveness of this predictive tool. All experiments were performed in the Anechoic Wind Tunnel (AWT) at the Hessert Center for Aerospace Research at the University of Notre Dame. The AWT was constructed in the early 1990s as part of the development of the Hessert Center for Aerospace Research. The anechoic chamber has a working space 6.1 m (20 ft) wide × 7.9 m (26 ft) long × 2.4 m (8 ft) high with 55.9-cm (22-in.) fiberglass sound-absorbing wedges on all six sides. This wedge configuration provides a low-frequency cutoff of about 100 Hz. Above the cutoff frequency, the wedges have a coefficient of energy absorption at normal incidence of 0.99 or greater. A low turbulence subsonic freejet test-section wind tunnel has been developed to fit into this anechoic chamber to accommodate aerodynamic and sound-pressure-level measurements generated from propellers, fans, pumps, airfoil configurations, etc. The cross-sectional area of the test region is 0.37 m^2 (4 ft^2) with a maximum velocity of about 30.5 m/s (100 ft/s). A complete description of the tunnel's individual components and important characteristics is presented in Mueller et al.[14,15]

The examination of the correlation length scale was one component of a larger study to examine the unsteady response of stator vanes located downstream of a propeller that was ingesting broadband turbulence.[16,17] Although a detailed discussion of the critical results of this study is beyond the scope of the current paper, the effort focused on distinguishing between different contributions to the turbulent flowfield that then interacted with the downstream stator. These contributions included the upstream turbulence ingested and modified by the propeller, the propeller wake, and propeller blade-tip vortices. Independent of the sources involved, flowfield measurements, using an X-wire, were used to define the turbulence spectra downstream of the propeller. It is this turbulence field that interacts with the stator, resulting in its aeroacoustic response. The data acquired in this manner are in the stator reference frame. As such, the spectra described in this paper represent a circumferential

average downstream of the propeller, corresponding to the flowfield "seen" by the stator vanes.

A photograph of the propeller/stator system integrated in the AWT is provided in Fig. 3. Freestream velocity travels through an upstream turbulence generation grid. This flow travels downstream through the propeller plane, where the grid-generated turbulence is modified by the movement and geometry of the propeller. In addition to this modification of the flow, the wake of the propeller changes the turbulent flow characteristics as well. These influences convect downstream and over a flat-plate airfoil, an idealized stator. The unsteady surface pressure (and thus the far-field acoustics) generated over the stator is the result of the unsteady flow seen by the airfoil. The coordinate system for this survey was a standard Cartesian system using primary directions of the flow and airfoil as reference points, as indicated in Fig. 4. For example, the primary (axial) flow direction in the system is represented by x_1. This also represents the chordwise direction of the stator when it is arranged at 0-deg angle of attack relative to the direction of the freestream flow upstream of the influence of the propeller. Likewise, the normal and spanwise direction of the stator in this orientation are also primary reference directions (x_2 and x_3), respectively. Note that this coordinate system is consistent with the theoretical arguments presented in Sec. II.

Fig. 3 Propeller/stator test rig mounted in Anechoic Wind Tunnel.

The propeller plane was located 0.61 m (2 ft) downstream of the turbulence generation grids, as the flow has been meticulously examined in this location for both turbulence grid conditions (with and without the presence of an upstream grid). Extensive studies[10,16] have shown that the grid-generated turbulence approaches isotropy in this plane displaying the quasi-isotropic behavior discussed in Sec. II.A. Key flow characteristics for cases with and without an upstream grid are presented in Table 1.

An appropriate length scale associated with the positioning of the stator downstream of the propeller is the maximum chord length of the rotor or propeller blade. At distances greater than one chord length, the influence of the unsteady pressure field from either the rotor or stator on its compliment can be ignored.[3,18,19] Therefore, the nose of the stator was positioned downstream of the propeller at an axial distance of one propeller chord from the propeller's trailing edge. In the study, three different propellers, composed of 4, 10, and 20 blades respectively, were used in order to examine the effect of blade spacing. The length scale of the four-bladed propeller is significantly larger than that of the 10- and 20-bladed propeller as a result of chord length differences.

A brief summary of operating conditions is given in Table 2. Operating conditions were selected to take advantage of prior experiments within the same facility.[10,16]

Velocity measurements were taken using an X-wire anemometry probe. The X-wire anemometry probe is, through proper calibration,

Table 1 Key characteristics of turbulence generation grid

Grid parameter	Clean flow	3-in. grid
Mesh size	N/A	7.62 cm (3.0 in.)
Rod diameter	N/A	0.953 cm (0.375 in.)
Grid solidity	0	0.33
RMS turbulence velocity	0.02 m/s (0.07 ft/s)	0.79 m/s (2.60 ft/s)
RMS turbulence intensity	0.15%	6.2%

Table 2 Summary of experimental operating conditions [freestream velocity 12.7 m/s (41.7 ft/s)]

Propeller	Loading condition	Advance ratio, J	BPF, Hz
4-bladed	Loaded	1.0	200
4-bladed	Unloaded	1.4	162
10-bladed	Loaded	1.14	550
10-bladed	Unloaded	1.31	480
20-bladed	Loaded	1.14	1100
20-bladed	Unloaded	1.31	960

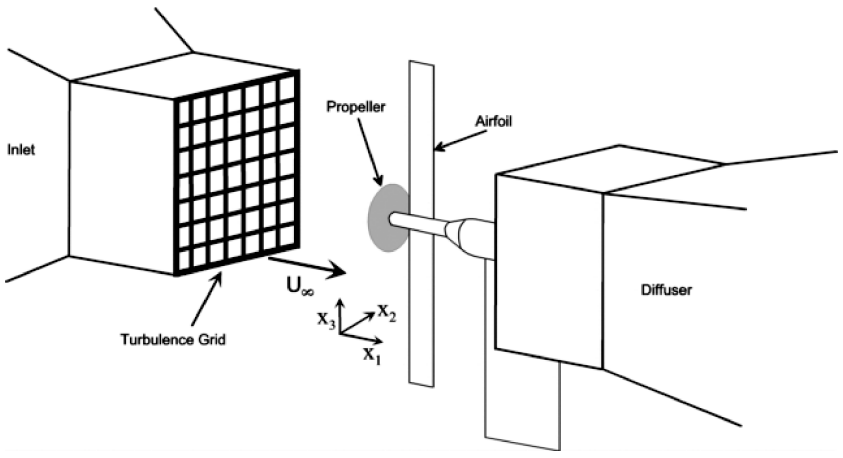

Fig. 4 Experimental setup for airfoil downstream of propeller ingesting broadband turbulence.

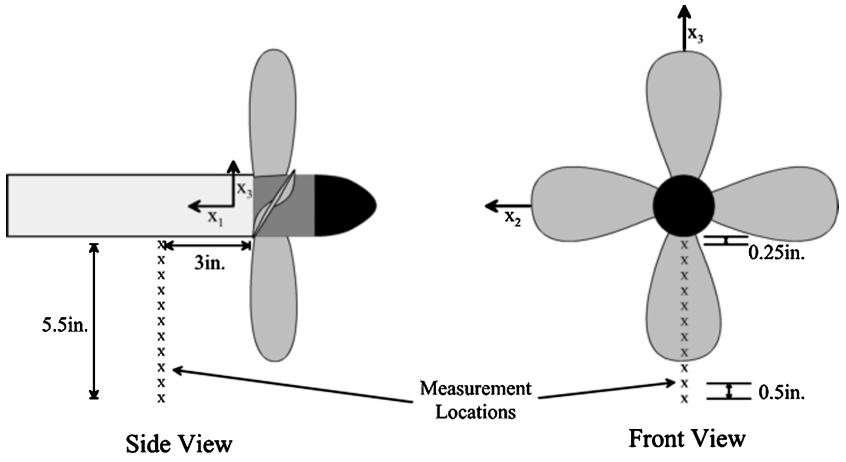

Fig. 5 Schematic of velocity measurement locations (four-bladed propeller locations shown).

able to measure two components of the velocity vector simultaneously. By phase-lock triggering data acquisition and manually rotating the probe 90 deg in the probe holder, all three components of the vector could be determined. Careful checking of the measurements in both the x_1–x_2 and x_1–x_3 planes, showing excellent matching of the x_1 component, suggested cross-contamination effects were minimal. For the velocity measurements, the downstream stators were removed so that the X-wire probe could be placed at the streamwise location corresponding to the leading edge of the stator. This turbulence characteristics at this point represent the turbulence driving the aeroacoustic response of the stator.

All measurement points involved 625 ensembles of 4096 samples taken at a sampling frequency of 8000 Hz. The locations of the measurements are explained in the schematic in Fig. 5, representing the measurement positions downstream of the four-bladed propeller. The chord length of the 10- and 20-bladed propeller was only 2.54 cm (1 in.), so that the streamwise position of these measurements was much closer to the trailing edge of the respective propellers. All measurements were made beneath the propeller dynamometer shaft and assumed to be equal at matching locations on the top of the dynamometer (top dead center of the propeller plane), which were the locations of the downstream stator vanes. Geometrical interference from the propeller dynamometer dictated a minimum radial distance from the center of the dynamometer hub. Therefore, measurements were made in 1.27-cm (0.5-in.) increments starting at a radial distance of 3.18 cm (1.25 in.) from the center of the dynamometer hub and continuing out to a distance of 15.9 cm (6.25 in.) from the center of the dynamometer hub. The outermost distances of each set were considered the freestream condition, as there was no evidence of propeller influence at these locations.

Twin X-wires were used in the determination of spanwise turbulence correlation length scale. The experimental method for determination of this correlation length scale is to take two velocity probes and measure the cross correlation between the two. Integrating this cross correlation from zero separation to a distance in which the correlation goes to zero gives the value for the correlation length scale. However, this was not done in the current investigation. These repeated correlation measurements for the range of separations needed would involve a significant amount of measurement and processing time. For the test matrix considered in this study (multiple points downstream of three different propellers, each with two different operating speeds, and different ingested turbulence conditions), the time involved would prevent the completion of other efforts more central to the research effort.

Rather than spend an inordinate amount of time focusing on this effort, an idea from Wojno[10] was incorporated into the current study. From Corcos[20] and Dryden,[21] an assumption of exponential spatial decay is assumed for the correlation of the turbulence. That is,

$$g(r_i) \approx e^{-r_i/\Lambda_i} \tag{44}$$

where $g(r_i)$ is the nondimensional lateral velocity correlation function, r_i is the spatial separation distance in the specified direction, and Λ_i is the correlation length scale. In terms of the actual experimental procedure, the equation can be rewritten as

$$\begin{aligned}\sqrt{\gamma^2(f,r_i)} &\equiv \left[\frac{\Phi_{u_{2_1}u_{2_2}}(f,r_i)\Phi^*_{u_{2_1}u_{2_2}}(f,r_i)}{\Phi_{u_{2_1}u_{2_1}}(f)\Phi_{u_{2_2}u_{2_2}}(f)}\right]^{\frac{1}{2}}\\ &= g(r_i)\\ &\approx e^{-|r_i|/\Lambda_3|_2}\end{aligned} \tag{45}$$

where γ^2 is the coherence function defined in terms of the turbulence crossspectra and autospectra, Φ_{ij} and Φ_{ii}, respectively. In the preceding equation, the primary subscript denotes a velocity direction (in this case, the normal or x_2 direction), and the secondary subscript denotes a probe number (1 or 2). In this way, the correlation length scale, which is frequency dependent, can be determined by measuring the coherence between two probes at a defined separation r_i (in this case, $i = 3$ for a spanwise separation), then solving for $\Lambda_3|_2$. Wojno found that in assuming this functional form, cases for a range of probe separations collapse to a uniform curve. A similar analysis was performed in the current study. The effectiveness of such an assumption is presented in Sec. IV.A.

IV. Experimental Results

The analysis and results described in this section were completed for the entire test matrix described in Sec. III. That is, the analysis was completed at all measurement locations downstream of all propellers at both loading conditions for each propeller. The results presented next are typical, but focus on only two measurement points in one propeller/loading condition, emphasizing analysis of the techniques rather than a discussion of all results in the matrix. A more thorough discussion is presented in Lynch.[16] The points considered for this discussion were measurements downstream of the four-bladed propeller in the "unloaded" condition ($J = 1.4$), located downstream of the 3-in. turbulence generation grid. One point was located 15.9 cm (6.25 in.) from the hub center, while the other was 7.0 cm (2.75 in.) from the hub center. These represent cases of the turbulence being a contribution from upstream sources only and a combination of propeller and upstream sources, respectively. In terms of the theory advanced in this discussion, they represent turbulent field cases of increasing complexity, from a quasi-isotropic case (upstream sources only) to a case where the turbulence is not only nonisotropic, but also inhomogeneous (propeller and upstream sources). This allows the theory's effectiveness over a broader range of applications to be considered. These cases are considered in Secs. IV.B and IV.C, respectively.

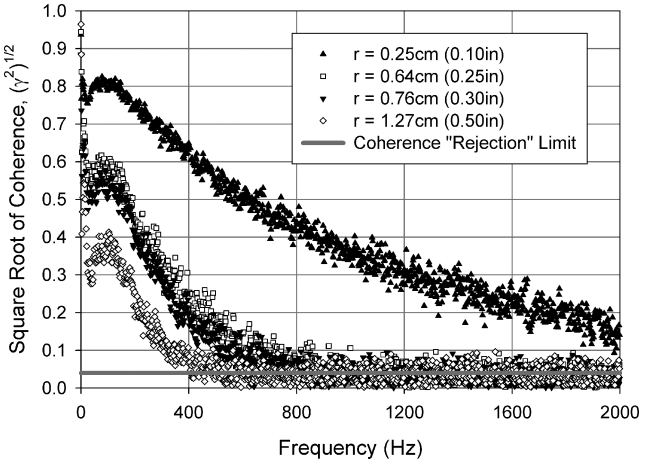

Fig. 6 Square root of coherence as a function of frequency and probe separation (upstream-turbulence-only location).

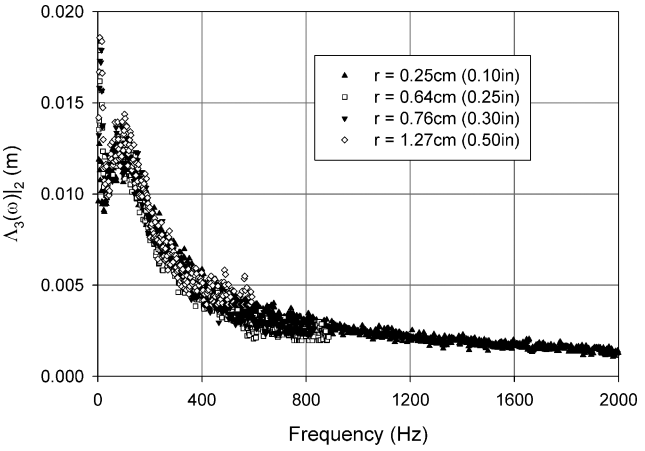

Fig. 7 Experimental estimation of correlation length scale $\Lambda_3|_2$ using exponential Corcos model for spatial correlation decay (upstream-turbulence-only location).

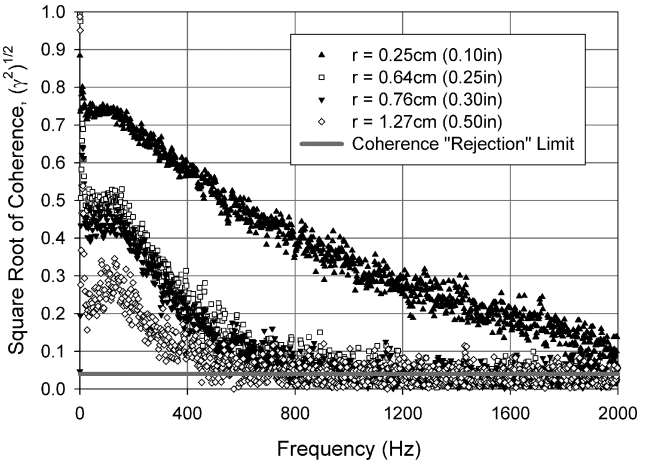

Fig. 8 Square root of coherence as a function of frequency and probe separation (propeller-generated and upstream-turbulence location).

A. Defining a Measure of Merit

To efficiently measure this correlation length scale, an exponential spatial decay model was assumed for the correlation of the turbulence. This approach mirrors the techniques employed by Corcos,[20] Dryden,[21] and Wojno,[10] and is explained in Sec. III. The model employs a coherence measurement between two probes separated by a distance r [see Eq. (45)]. The square root of coherence is plotted as a function of frequency for a range of separation distances in Fig. 6 at the "upstream turbulence only" location. Note that the separation distances required between the two probes are quite small, increasing the difficulty in the measurements. A benefit to the technique presented in this paper is that all necessary measurements are single point, thereby requiring only one probe.

Returning to Fig. 6, the effectiveness of the Corcos model would be reflected in the collapse of coherence measurements to a single curve in the calculation of correlation length. However, even at small separation distances the coherence between probes quickly falls to zero, especially for small scales of turbulence (reflected in higher frequencies). Bendat and Piersol[22] and Wojno[10] conclude that the resolution of the coherence measurements can be described as

$$\Delta\sqrt{\gamma^2} \sim 1/\sqrt{N} \tag{46}$$

where N is the number of ensembles taken (625 for these tests). This gives a $\Delta\sqrt{\gamma^2}$, or resolution, of 0.04. Therefore, if the square root of the coherence is less than that value, it is statistically zero and removed from consideration. This is reflected in the coherence "rejection" line shown in Fig. 6.

The results of application of this technique are shown in Fig. 7. Although the cleanest, most informative data are represented by the smallest separation, the curves from all separations considered appear to collapse to a uniform curve in the calculation of length scale, within the uncertainty of the experiment ($\pm 10\%$) for almost all data points.

The same approach is now applied to the highly nonisotropic case downstream of the propeller. As stated earlier, the turbulent field here is the result of the upstream turbulence already presented, combined with complex influence of the rotating propeller. Before applying the correlation length scale theory of Sec. II, a measure of merit must be defined. Using the same probe separations, coherence between the probes for the turbulence in the x_2 direction was measured. These results are presented in Fig. 8. Using the length-scale estimation technique and ignoring points whose values were below the floor level defined by the rejection limit, these results also collapse to a uniform curve, as shown in Fig. 9.

B. Quasi-Isotropic Turbulence Case

There now exists some measure of merit for the predicted correlation length scale expression given in Eq. (40). The first case considered is at a position that is representative of turbulence contributions from only the upstream grid. Wojno[10] showed that this grid-generated turbulence reaches a nearly isotropic state at the propeller plane. Lynch[16] concluded that there is no quantifiable influence from the propeller at this measurement location, based on comparison of the mean velocity and turbulence spectra for run conditions with and without the propeller. As such, it represents the "simplest" case for the model. Figure 10 compares the experimental data set formed by the combination of separation distances depicted in Fig. 7 with the function generated using Eq. (40). With isotropy, $\alpha_c \sim 1$, and the key parameter is Λ. Using Eq. (33), Λ is determined using the streamwise turbulence energy spectrum, taking the limit as $k_c \to 0$. In this case, Λ was calculated to be 1.8 cm (0.70 in.). Results are plotted as a function of nondimensional wave number, requiring a conversion to the spatial domain using a frozen-field assumption (recall from Sec. II.A that $k_1 = k_c$). As is clearly seen, the prediction based only on integral length scale is in excellent agreement with experimental data. In fact, when considering Figs. 6–10, the most significant departures between the prediction and experimental results comes from the experimental data contributed by the largest separation between probes, where coherence values are small. For the better data sets associated with smaller separations, the agreement is excellent.

C. Nonisotropic Turbulence Case

The turbulent flowfield is much more complex in the region influenced by the propeller. The details are beyond the scope of this paper (but are discussed in detail in Lynch[16] and Lynch et al.[23,24]). Basically, the flowfield over most of the region influenced by the propeller (away from hub and tip effects) is the result of superposition of

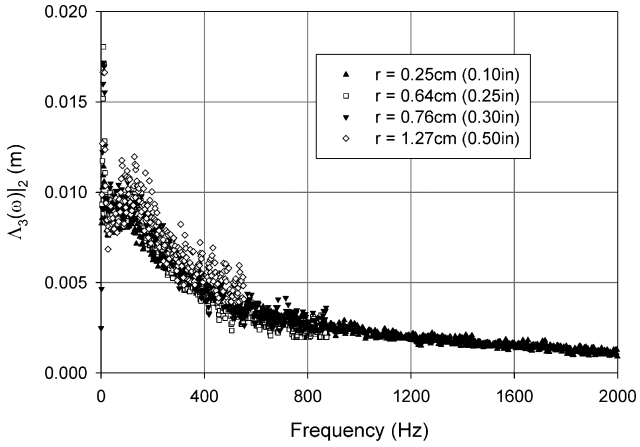

Fig. 9 Experimental estimation of correlation length scale $\Lambda_3|_2$ using exponential Corcos model for spatial correlation decay (propeller-generated and upstream-turbulence location).

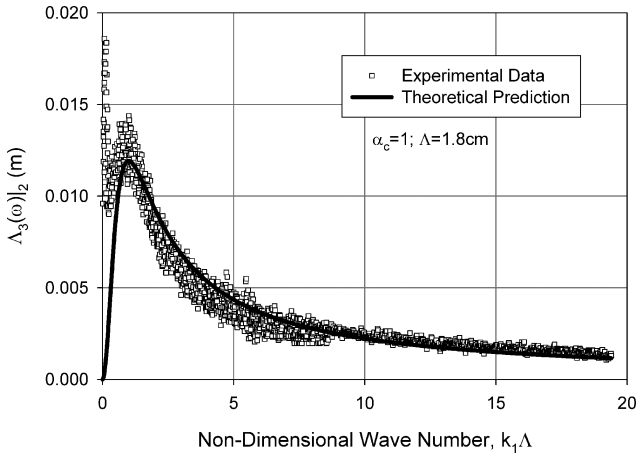

Fig. 10 Comparison of experimentally estimated and predicted correlation length scale $\Lambda_3|_2$ (upstream-turbulence-only location).

contributions from 1) propeller wakes and 2) ingested turbulence, which is modified by the propeller. Models developed in Lynch et al.[23,24] capture the relative levels of these contributions, but in terms of the response of the downstream stator the total turbulence is the quantity of interest. Still, there are a number of important results from the modeling of contributions that could affect correlation length scale. The broadband contribution of the propeller wake dominates spectral levels at high frequencies. However, at low frequencies the propeller geometry works to suppress the largest scales of ingested turbulence. The result is a smaller turbulence integral length scale [measured as 1.2 cm (0.5 in.)], which should manifest itself in a corresponding decrease in spanwise correlation scale (assuming the two are indeed related). Further, it is unrealistic to assume that the turbulence is still accurately represented with an isotropic assumption.

The same analysis as the upstream-turbulence-only case was used on a point influenced by the presence of a propeller. The only changes in the analysis were the artificial removal of tonal peaks in the spectrum associated with wakes passing the sensor at harmonics of blade passage frequency (BPF) and the consideration of anisotropy as it relates to the coordinate stretching factor α_c taken as 0.8 in this case. This reflects the slight stretching of eddies in the streamwise direction compared to the spanwise direction, as experimentally determined in Lynch.[16] The results are shown in Fig. 11. Again, although not specifically shown in this case, the most significant disagreement between theory and experimental data occurred with the experimental data contribution of the largest probe separation. Note that the values of the length scale reflect the expected decrease caused by a decrease in integral length scale.

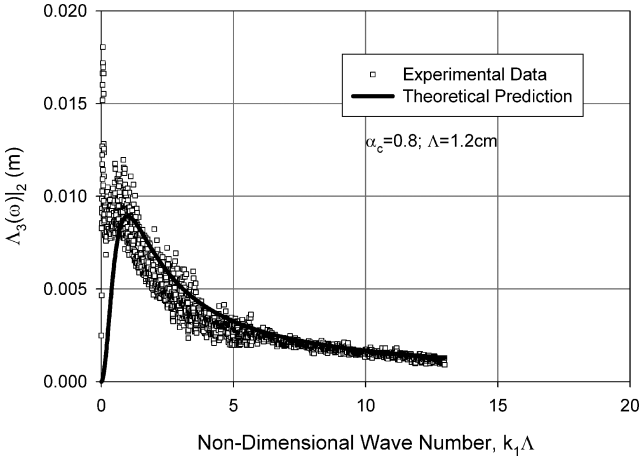

Fig. 11 Comparison of experimentally estimated and predicted correlation length scale $\Lambda_3|_2$ (propeller-generated and upstream-turbulence location).

D. Aeroacoustic Response Prediction Based on Correlation Length Scale

As the predicted correlation length scales closely reflect those experimentally estimated, a demonstration can be made as to the effectiveness of the tool to contribute to the formula presented in Eq. (1) for prediction of the acoustic contribution of the stator. The effective modeling of correlation length scale is highly encouraging as a tool to now be used to predict the acoustic output of the system.

Again focusing the consideration to the broadband turbulence field responsible for the unsteady response of the stator, the stator pair pictured in Fig. 3 can be divided into two primary sections. These sections are the spanwise regions affected by unmodified grid-generated turbulence and those affected by propeller-modified turbulence. Analysis of the propeller-modified turbulence field suggests that, with proper nondimensionalization by local values of variables such as rms turbulence intensity and freestream velocity, the propeller-modified field could be represented by the measurements at one point.[16] That is, the nondimensionalized turbulence quantities downstream of the propeller were basically uniform in terms of the broadband turbulence (with the exception of the regions near the hub and near the passing tip vortices). Therefore, the prediction of the acoustic output from the stators could be made using one point that represents grid-generated turbulence and one point that represents propeller-modified turbulence, represented in the analysis of Secs. IV.B and IV.C, respectively. These two models would then be applied over the length of the stator to which each turbulence field applied [the term L_3 in Eq. (1)]. As Scharpf[25] noted that the stream tube changes for the four-bladed propeller were negligible, it was decided that the simple geometry provided a satisfactory approximation for these lengths of influence. Specifically, the length of interest for the propeller-modified turbulence was equal to the diameter of the given propeller (minus the diameter of the dynamometer hub), whereas the length of interest for the unmodified grid-generated turbulence was the difference between the tunnel width and the propeller diameter. Application of the appropriate lengths and length scales gives a prediction for the acoustic output of the stator.

For the case considered, there were numerous contributions to the overall radiated acoustic field, including background tunnel levels, the upstream turbulence grid, the propeller's self-noise and response to its ingested turbulence field, the stator self-noise, and the stator's response to its ingested turbulence field. The purpose of this effort is not the prediction of the acoustic output of the propeller, which has been developed in prior efforts at the University of Notre Dame.[26–29] As the analysis of the majority of these contributions was beyond the scope of the study (and certainly beyond the scope of this paper), all but the stator's response to its ingested turbulence field were determined experimentally. Assuming no correlation between individual sources, relative levels could be determined through selective

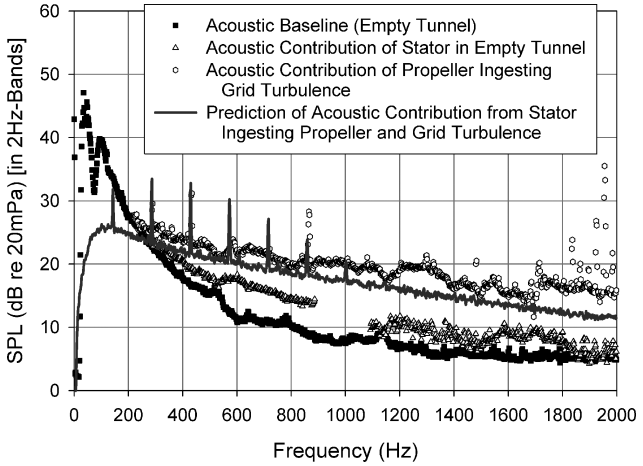

Fig. 12 Breakdown of contributions to the radiated acoustic spectrum [four-bladed propeller behind 3-in. grid, unloaded case ($J = 1.4$)].

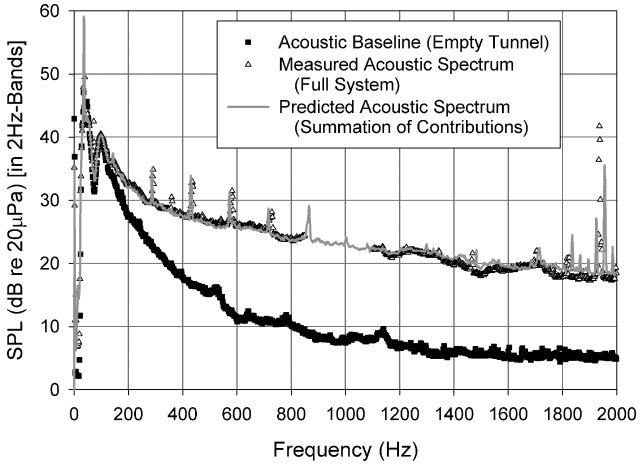

Fig. 13 Comparison of predicted and experimentally measured acoustic output of the propeller/stator system for four-bladed propeller behind 3-in. grid, unloaded case ($J = 1.4$).

elimination of components and power summation techniques. The result is a breakdown like that shown in Fig. 12, which compares the relative contributions to the acoustic field. Over a substantial part of the spectrum considered, the predicted levels of the stator's response to ingested turbulence represents a significant contribution to the radiated acoustic field. In the frequency range between 900–1100 Hz, the spectra involving the stator were found to be dominated by stator trailing-edge noise,[16] which is not included in the theoretical models described here. Therefore, this region was artificially suppressed for clarity.

The contributions can then be power summed to develop a prediction for the radiated acoustic field generated by the entire system. Figure 13 shows this result compared to measured levels. Over the entire frequency range of interest, the theoretical curve accurately predicts the measured value, including the peaks associated with the BPF harmonics. The unsteady response of the stator to the ingested turbulence field represents a substantial influence in the radiated acoustic spectrum. Therefore, because the correlation length scale is an important parameter in such a prediction the importance of the scale's accurate prediction is emphasized. In this case, the prediction is impressive not only for the ability of the length scale estimation given in Sec. II to predict the acoustic output, but also that this output prediction is based on turbulence measurements at only two locations. Although this paper considers only one propeller loading, similar results were found for all propellers and loading conditions considered in this study.[16]

V. Conclusions

This paper provides a derivation of correlation length scale as a function of classic turbulence integral length scale. The benefit of such a tool is that such a scale, traditionally determined utilizing an array of two-point correlation measurements, can be determined using relatively simple one-point measurements. Its utility is illustrated in the accurate estimation of the aeroacoustic response of a stator to a turbulent flowfield.

Acknowledgments

This research was performed at the Hessert Center for Aerospace Research of the Department of Aerospace and Mechanical Engineering at the University of Notre Dame. The work was supported by the U.S. Navy, Office of Naval Research, located in Arlington, Virginia, under Contracts N00014-99-1-0284 and N00014-01-1-0424. The Program Manager was L. Patrick Purtell.

References

[1]von Kármán, T., and Sears, W. R., "Airfoil Theory for Non-Uniform Motion," *Journal of the Aeronautical Sciences*, Vol. 5, No. 10, 1938, pp. 379–390.

[2]Sears, W. R., "Some Aspects of Non-Stationary Airfoil Theory and Its Practical Application," *Journal of the Aeronautical Sciences*, Vol. 8, No. 3, 1941, pp. 104–108.

[3]Blake, W. K., *Mechanics of Flow Induced Sound and Vibration*, Wiley, New York, 1986.

[4]Amiet, R. K., "Acoustic Radiation from an Airfoil in a Turbulent Stream," *Journal of Sound and Vibration*, Vol. 41, No. 4, 1975, pp. 407–420.

[5]Wygnanski, I., Champagne, F., and Marasli, B., "On the Large-Scale Structures in Two-Dimensional Small-Deficit, Turbulent Wakes," *Journal of Fluid Mechanics*, Vol. 168, 1986, pp. 31–71.

[6]Glegg, S. A. L., "Prediction of Blade Wake Interaction Noise Based on a Turbulent Vortex Model," *AIAA Journal*, Vol. 29, No. 10, 1991, pp. 1545–1551.

[7]Devenport, W. J., Wenger, C. W., Glegg, S. A. L., and Miranda, J. A., "Wave Number Frequency Spectra of a Lifting Wake for Broadband Noise Prediction," *AIAA Journal*, Vol. 36, No. 6, 1998, pp. 881–887.

[8]Devenport, W. J., Muthanna, C., Ma, R., and Glegg, S. A. L., "Two-Point Descriptions of Wake Turbulence with Application to Noise Prediction," *AIAA Journal*, Vol. 39, No. 12, 2001, pp. 2302–2307.

[9]Glegg, S. A. L., Wittmer, K. S., Devenport, W. J., and Pope, D. S., "Broadband Helicopter Noise Generated by Blade Wake Interactions," *Journal of the American Helicopter Society*, Vol. 44, No. 4, 1999, pp. 293–301.

[10]Wojno, J. P., "An Experimental Investigation of the Aeroacoustic Response of a Ten-Bladed Rotor Ingesting Grid-Generated Turbulence," Ph.D. Dissertation, Dept. of Aerospace and Mechanical Engineering, Univ. of Notre Dame, Notre Dame, IN, 1999.

[11]Panton, R. L., and Linebarger, J. H., "Wall Pressure Spectra Calculations for Equilibrium Boundary Layers," *Journal of Fluid Mechanics*, Vol. 65, No. 2, 1974, pp. 261–287.

[12]Hinze, J. O., *Turbulence*, McGraw–Hill, New York, 1975.

[13]Gradshteyn, I. S., and Ryzhik, I. M., *Table of Integrals, Series, and Products*, Academic Press, New York, 1980.

[14]Mueller, T. J., Scharpf, D. F., Batill, S. M., Strebinger, R. B., Sullivan, C. J., and Subramanian, S., "The Design of a Low-Noise, Low-Turbulence Wind Tunnel for Acoustic Measurements," AIAA Paper 92-3883, July 1992.

[15]Mueller, T. J., Scharpf, D. F., Batill, S. M., Strebinger, R. B., Sullivan, C. J., and Subramanian, S., "A New Low Speed Wind Tunnel for Acoustic Measurements," *Proceedings of the European Forum on Wind Tunnels and Wind Tunnel Test Techniques*, Royal Aeronautical Society, London, 1992.

[16]Lynch, D. A., III, "An Experimental Investigation of the Unsteady Response of a Stator Located Downstream of a Propeller Ingesting Broadband Turbulence," Ph.D. Dissertation, Dept. of Aerospace and Mechanical Engineering, Univ. of Notre Dame, Notre Dame, IN, 2001.

[17]Lynch, D. A., III, Mueller, T. J., and Blake, W. K., "Aeroacoustic Response of an Airfoil Downstream of a Propeller Ingesting Broadband Turbulence," AIAA Paper 2001-2240, May 2001.

[18]Kaji, S., and Okazaki, T., "Generation of Sound by Rotor-Stator Interaction," *Journal of Sound and Vibration*, Vol. 13, No. 3, 1970, pp. 281–307.

[19]Falk, E. A., "An Experimental Investigation of Aerodynamic Forcing in the F109 Turbofan Engine Compressor," Ph.D. Dissertation, Dept. of Aerospace and Mechanical Engineering, Univ. of Notre Dame, Notre Dame, IN, 2000.

[20]Corcos, G. M., "The Structure of the Turbulent Pressure Field in Boundary-Layer Flows," *Journal of Fluid Mechanics*, Vol. 18, 1964, pp. 353–378.

[21]Dryden, H. L., "Turbulence Investigations at the National Bureau of Standards," *Proceedings of the 5th International Congress of Applied Mathematics*, 1938.

[22]Bendat, J. S., and Piersol, A. G., *Random Data: Analysis and Measurement Procedures*, Wiley, New York, 2000.

[23]Lynch, D. A., III, Blake, W. K., and Mueller, T. J., "Turbulent Flow Downstream of a Propeller, Part 1: Wake Turbulence," *AIAA Journal*, Vol. 43, No. 6, 2005, pp. 1198–1210.

[24]Lynch, D. A., III, Blake, W. K., and Mueller, T. J., "Turbulent Flow Downstream of a Propeller, Part 2: Ingested, Propeller-Modified Turbulence," *AIAA Journal*, Vol. 43, No. 6, 2005, pp. 1211–1220.

[25]Scharpf, D. F., "An Experimental Investigation of the Sources of Propeller Noise Due to Turbulence Ingestion," Ph.D. Dissertation, Dept. of Aerospace and Mechanical Engineering, Univ. of Notre Dame, Notre Dame, IN, 1993.

[26]Minniti, R. J., III, Blake, W. K., and Mueller, T. J., "Inferring Propeller Inflow and Radiation from Near-Field Response, Part 1: Analytic Development," *AIAA Journal*, Vol. 39, No. 6, 2001, pp. 1030–1036.

[27]Minniti, R. J., III, Blake, W. K., and Mueller, T. J., "Inferring Propeller Inflow and Radiation from Near-Field Response, Part 2: Empirical Application," *AIAA Journal*, Vol. 39, No. 6, 2001, pp. 1037–1046.

[28]Wojno, J. P., Mueller, T. J., and Blake, W. K., "Rotor Turbulence Ingestion Noise, Part 1: Experimental Characterization of Grid-Generated Turbulence," *AIAA Journal*, Vol. 40, No. 1, 2002, pp. 16–25.

[29]Wojno, J. P., Mueller, T. J., and Blake, W. K., "Rotor Turbulence Ingestion Noise, Part 2: Rotor Aeroacoustic Response," *AIAA Journal*, Vol. 40, No. 1, 2002, pp. 26–32.

H. Atassi
Associate Editor